

METHODOLOGICAL NOTES

PACS numbers: 42.55.Ye, 42.65.Dr, 42.65.Ky, 42.70.Mp, 42.79.Nv

Parametric coupling of frequency components at stimulated Raman scattering in solids

T T Basiev, S N Smetanin, A S Shurygin, A V Fedin

DOI: 10.3367/UFNe.0180.201006f.0639

Contents

Abstract. **We analyze the effect of parametric coupling of different frequency components at the stimulated Raman scattering threshold depending on the four-wave mixing phase mismatch and material dispersion. A fundamental difference is observed in the way parametric processes affect the generation of Stokes and anti-Stokes waves. We show that as a result of parametric coupling of Stokes components, their generation thresholds strongly decrease and come closer to each other because they originate from an intense parametric rather than a spontaneous seed radiation. The theoretical analysis refines and extends the commonly accepted concept of stimulated Raman scattering in nonlinear crystals and demonstrates good agreement with new experimental data.**

1. Introduction

Nonlinear-optical conversion of solid-state laser radiation is a widely accepted method of shifting laser radiation frequencies to the spectral domains where direct lasing is hindered. Stimulated Raman scattering (SRS) in crystals and optical fibers enables making compact solid-state SRS lasers (see review Refs [1 – 6]) with radiation wavelengths shifted to the infrared radiation domain (which is not harmful to the eye), to the atmospheric and optical fiber 'transparency windows,' up to the transparency edge of the SRS-active material [7].

T T Basiev Prokhorov General Physics Institute,
Russian Academy of Sciences,
ul. Vavilova 38, 119991 Moscow, Russian Federation
Tel. (7-499) 135 02 67
E-mail: basiev@lst.gpi.ru
S N Smetanin, A S Shurygin, A V Fedin Degtyarev Kovrov State Technological Academy,
ul. Mayakovskogo, 601910 Kovrov, Vladimir region, Russian Federation
Tel. (7-49232) 3 13 47
E-mail: ssmetanin@bk.ru

Received 3 December 2009, revised 21 April 2010
Uspekhi Fizicheskikh Nauk **180** (6) 639 – 646 (2010)
DOI: 10.3367/UFNr.0180.201006f.0639
Translated by E N Ragozin; edited by A M Semikhatov

SRS conversion in solids, which has been much studied in the visible range, proceeds in a cascade-like manner, or step-by-step, in the absence of other nonlinear effects [8, 9]. But the realization of infrared cascade-like generation of higher Stokes SRS radiation components is strongly hindered by a considerable decrease in the SRS gain coefficient with increasing the wavelength [10] and is limited in intensity by the radiation damage threshold of the SRS medium. At the same time, it must be taken into account that the dispersion of the refractive index in the majority of solids becomes substantially weaker with further advancement to the infrared region. This increases the nonlinear wave interaction length and enhances the accompanying nonlinear effects, which require the phase matching condition to be satisfied. Among the attendant nonlinear effects, we note four-wave mixing (FWM), which is responsible for the parametric coupling of SRS components. Both Stokes and anti-Stokes radiation components can be generated under this Raman-parametric conversion in solids (see review Refs [8, 9]).

The parametric coupling of SRS components, which was first observed by Terhune [11] in 1963, at the dawn of nonlinear optics, led to the conical emission of anti-Stokes waves in materials with a strong dispersion. At that time, Terhune [12] and several other authors [13 – 16] interpreted these results based on the notion of a partly degenerate FWM among the laser (wave vector $\mathbf{k}_{\text{laser}}$), the first Stokes (wave vector $\mathbf{k}_{\text{S}}$), and the first anti-Stokes (wave vector $\mathbf{k}_{\text{aS}}$) waves obeying the vector phase matching condition $2\mathbf{k}_{\text{laser}} = \mathbf{k}_{\text{S}} + \mathbf{k}_{\text{aS}}$. The mechanism of simultaneous conical emission of higher anti-Stokes and Stokes SRS components obeying the exact FWM phase matching conditions was also qualitatively discussed in those papers. The rigorous theory of FWM in SRS was constructed only for the conical emission of anti-Stokes waves [17], and now this effect is widely used in Raman spectroscopy, as the method of coherent anti-Stokes Raman scattering (CARS) (see review Ref. [18]).

In later experimental studies, the axial emission of anti-Stokes waves in SRS was also observed, and was interpreted in the framework of a model involving the spatially bounded capture of the phases of parametrically coupled waves [19]. The anti-Stokes lasing of solid-state SRS lasers [20, 21], realized with an efficiency $< 1\%$, may also be attributed to the spatially bounded phase capture.

In Ref. [7], a single-pass mid-infrared SRS conversion of 1.56 and 1.91 μm laser radiation was investigated experimentally in a cubically nonlinear $BaWO_4$ crystal, which is optically transparent to wavelengths up to 3.7 μm. For the first time, the authors of Ref. [7] were able to obtain a record-long wavelength of SRS in the mid-infrared range 3.69 μm (the fourth Stokes component). They also noted that one of the reasons for low-threshold lasing may be the occurrence of four-wave parametric processes due to the weak dispersion of the refractive index of the $BaWO_4$ SRS crystal in the mid-infrared range.

It was determined in Refs [22, 23] that the use of a $Ba(NO_3)_2$ SRS crystal, which exhibits a strong dispersion of the refractive index [24], and 1.064 μm radiation pumping has the effect that the lasing thresholds of the Stokes components differ greatly. This is an indication that the SRS is cascade-like in character. When a $BaWO_4$ SRS crystal is used, which exhibits a weaker dispersion in the infrared region [25], the lasing thresholds of SRS components are quite close to each other, which may be attributed to their parametric coupling.

Therefore, despite the availability of rather voluminous literature on the theory and experimental realization of SRS in solids with material dispersion, the problem of the effect of four-wave nonlinear interactions on SRS remains to be fully explored. Although all equations describing these processes are known, their analysis, especially in the mid-infrared range with its weak material dispersion, is insufficient and the implications are obscure.

In this methodological paper, we therefore theoretically analyze the parametric four-wave coupling of the frequency radiation components in the SRS in solids in relation to the wave mismatch of parametric four-wave mixing, which is determined by the dispersion of the refractive index and the SRS medium length. Proceeding from our theoretical analysis and a comparison of its results with experimental data, we make suggestions concerning the optimal choice of nonlinear media and pump frequencies for the realization of low-threshold SRS in the mid-infrared range.

2. Theoretical description of the parametric coupling of SRS components

As shown in Refs [8, 14, 17], the contribution of parametric coupling to SRS depends on the fulfillment of the wave matching condition of partly degenerate FWM,

$$2\mathbf{k}_j = \mathbf{k}_{j-1} + \mathbf{k}_{j+1}\,, \tag{1}$$

where j is the number of an SRS component, which is an FWM pump wave ($j < 0$ is an anti-Stokes wave, $j > 0$ is a Stokes wave, and $j = 0$ is the SRS pump wave), $\mathbf{k}_j$ is the wave vector of the FWM pump, and $\mathbf{k}_{j-1}$ and $\mathbf{k}_{j+1}$ are the vectors of the neighboring SRS components, which are the signal and idle waves of FWM. We emphasize that the SRS pump ($j = 0$) and the FWM pump waves do not coincide in general. The existence of a wave mismatch,

$$\Delta k_j = k_{j-1} + k_{j+1} - 2k_j\,, \tag{2}$$

where k_j, k_{j-1}, and k_{j+1} are the moduli of the corresponding wave vectors, results in a violation of condition (1) in the case of axial (collinear) generation of SRS components, which weakens their parametric coupling.

The main cause of wave mismatch (2) is the dispersion of the refractive index of the medium. The wave mismatch is defined as (we assume that $k_j = 2\pi n_j \lambda_j^{-1}$ and $\lambda_j = (\lambda_0^{-1} - j\nu_R)^{-1}$)

$$\Delta k_j = (n_{j-1} + n_{j+1} - 2n_j)\,2\pi\lambda_j^{-1} + (n_{j-1} - n_{j+1})\,2\pi\nu_R\,, \tag{3}$$

where λ_j is the FWM pump wavelength, ν_R is the Raman frequency shift, and n_j, n_{j-1}, and n_{j+1} are the respective refractive indices of the FWM pump, signal, and idle waves.

Apart from the partly degenerate FWM, a nondegenerate FWM also occurs in SRS, such that the wave matching $\mathbf{k}_j + \mathbf{k}_{j+1} = \mathbf{k}_{j-1} + \mathbf{k}_{j+2}$ is satisfied [8, 14, 17], with the mismatch

$$\Delta K_j = \Delta k_j + (n_j + n_{j+2} - 2n_{j+1})\,2\pi\lambda_j^{-1} + (n_{j+1} - n_{j+2})\,4\pi\nu_R \approx \Delta k_j + \Delta k_{j+1}$$

significantly (approximately two times) greater than Δk_j, and we therefore neglect the nondegenerate FWM in our treatment. However, we note that the inclusion of all kinds of FWM in SRS in solids is required in the case where the SRS pump wavelength is close to the zero dispersion wavelength, which corresponds to the inflection point of the spectral dependence of the refractive index of a solid (the Sellmeier formula [26]), because all wave mismatches are then close to zero.

Another cause of the weakening of the parametric coupling of SRS components is the nonlinear self-action of weak signal and idle waves in the field of a strong FWM pump wave. In this case, the phases of the weak waves vary linearly as functions of the longitudinal coordinate z. This is equivalent to a constant addition to the magnitude of the wave vector of the weak wave, which violates the collinear wave matching condition of FWM [27].

The system of wave equations describing the parametrically coupled collinear SRS can be written as [28]

$$\frac{dE_{-1}}{dz} = i\,\frac{2\pi\omega_{-1}^2}{c^2 k_{-1}}\left[\chi_{-1}^*|E_0|^2 E_{-1} + \chi_{aS-S} E_0^2 E_1^* \exp(i\Delta k_0 z)\right],$$

$$\frac{dE_0}{dz} = i\,\frac{2\pi\omega_0^2}{c^2 k_0}\left(\chi_0^*|E_1|^2 E_0 + \chi_{-1}|E_{-1}|^2 E_0\right), \tag{4}$$

$$\frac{dE_1}{dz} = i\,\frac{2\pi\omega_1^2}{c^2 k_1}\left[\chi_0|E_0|^2 E_1 + \chi_{S-aS} E_0^2 E_{-1}^* \exp(i\Delta k_0 z)\right],$$

where c is the speed of light, E_j are the slowly varying complex amplitudes of the SRS pump wave ($j = 0$), anti-Stokes ($j = -1$), and Stokes ($j = 1$) waves, ω_j are their frequencies, χ_{-1} and χ_0 are the Raman susceptibilities for the corresponding waves, and χ_{aS-S} and χ_{S-aS} are the susceptibilities for the Raman-parametric coupling between the anti-Stokes and Stokes waves. The terms proportional to the Raman susceptibilities χ_{-1} and χ_0 describe the SRS amplification of the corresponding SRS components. The terms proportional to the complex conjugate Raman susceptibilities χ_{-1}^* and χ_0^* describe the depletion of the current SRS component in the SRS conversion to the next SRS component. The terms proportional to χ_{aS-S} and χ_{S-aS} describe the FWM in the SRS, while the exponential factors determine the FWM wave mismatch due to dispersion of the refractive index.

In what follows, we temporarily neglect the dispersion of Raman susceptibilities, i.e., we assume that $\chi_{-1} \approx \chi_0$; then $\chi_{\mathrm{aS-S}} \approx \chi^*_{-1}$ and $\chi_{\mathrm{S-aS}} \approx \chi_0$. We introduce the SRS gain coefficient for the Stokes wave [28] as

$$g = -\frac{4\pi\omega_1}{c^2 k_1}\,\mathrm{Im}\chi_0\,. \tag{5}$$

Because only the imaginary parts of the susceptibilities participate in the transformation of amplitudes, the system of equations can be written in a form more convenient for our analysis:

$$\begin{aligned}
\frac{\mathrm{d}E_{-1}}{\mathrm{d}z} &= -\frac{g}{2}\frac{\lambda_0}{\lambda_{-1}}\,E_0\left[E_0^* E_{-1} + E_1^* E_0 \exp\left(\mathrm{i}\Delta k_0 z\right)\right],\\
\frac{\mathrm{d}E_0}{\mathrm{d}z} &= -\frac{g}{2}\frac{\lambda_1}{\lambda_0}\,E_1 E_1^* E_0 + \frac{g}{2}\,E_{-1}E_{-1}^* E_0\,,\\
\frac{\mathrm{d}E_1}{\mathrm{d}z} &= \frac{g}{2}\,E_0\left[E_0^* E_1 + E_{-1}^* E_0 \exp\left(\mathrm{i}\Delta k_0 z\right)\right].
\end{aligned} \tag{6}$$

The initial conditions for system of equations (6) are given by

$$\begin{aligned}
&E_{-1}(0) = 0\,, \quad E_0(0) = \sqrt{I_0}\exp\left(\mathrm{i}\varphi_0\right),\\
&E_1(0) = \sqrt{S}\exp\left(\mathrm{i}\varphi_1\right),
\end{aligned} \tag{7}$$

where I_0 is the input SRS pump radiation intensity and S is the spontaneous Raman scattering intensity ($S \ll I_0$).

The analytic solution of system of equations (6) for an undepleted pump radiation $E_0(z) = E_0(0)$ is well known [16], and in the case of the FWM wave matching ($\Delta k_0 = 0$), this solution can be written in the form

$$\begin{aligned}
E_{-1}(z) &= \frac{\sqrt{S}}{\lambda_{-1}/\lambda_0 - 1}\exp\left[-\frac{g}{2}\,I_0 z\left(\frac{\lambda_0}{\lambda_{-1}} - 1\right)\right]\\
&\quad\times\exp\left[\mathrm{i}(2\varphi_0 - \varphi_1 \pm \pi)\right],\\
E_1(z) &= \frac{\sqrt{S}}{\lambda_{-1}/\lambda_0 - 1}\\
&\quad\times\left\{\frac{\lambda_{-1}}{\lambda_0}\exp\left[-\frac{g}{2}\,I_0 z\left(\frac{\lambda_0}{\lambda_{-1}} - 1\right)\right] - 1\right\}\exp\left(\mathrm{i}\varphi_1\right),
\end{aligned} \tag{8}$$

where the phase of the E_{-1} wave is $\varphi_{-1} = 2\varphi_0 - \varphi_1 \pm \pi$. In this case, the generalized phase of FWM [8, 19] is defined as $\Psi_0 = 2\varphi_0 - \varphi_{-1} - \varphi_1 = \pm\pi$. A shift of the generalized phase by π is responsible for the coherent subtraction of the parametrically converted waves and the absence of SRS generation of Stokes and anti-Stokes waves for $\Delta k_0 = 0$, which is well known in the theory of Stokes and anti-Stokes wave coupling in SRS [9]. Solutions (8) demonstrate an exponential attenuation of these waves (exponentials of a negative argument proportional to z).

The phase conditions of the parametric coupling of other SRS components not involving anti-Stokes waves have not been investigated until recently. The Raman-parametric coupling of any other three SRS components can be described by a system of equations similar to (6). To describe the coupling of the SRS pump E_0 and the first (E_1) and second (E_2) Stokes waves, we should increase all the numerical subscripts in (6) by unity; then the new system of equations is written as

$$\begin{aligned}
\frac{\mathrm{d}E_0}{\mathrm{d}z} &= -\frac{g}{2}\frac{\lambda_1}{\lambda_0}\,E_1\left[E_1^* E_0 + E_2^* E_1 \exp\left(\mathrm{i}\Delta k_1 z\right)\right],\\
\frac{\mathrm{d}E_1}{\mathrm{d}z} &= -\frac{g}{2}\frac{\lambda_2}{\lambda_1}\,E_2 E_2^* E_1 + \frac{g}{2}\,E_0 E_0^* E_1\,,\\
\frac{\mathrm{d}E_2}{\mathrm{d}z} &= \frac{g}{2}\,E_1\left[E_1^* E_2 + E_0^* E_1 \exp\left(\mathrm{i}\Delta k_1 z\right)\right].
\end{aligned} \tag{9}$$

For an undepleted pump, the first equation in (9) can be replaced by the equation $E_0(z) = \sqrt{I_0}\exp(\mathrm{i}\varphi_0)$. In the second equation, the first term in the right-hand side, which describes the depletion of E_1 in the conversion to E_2, can be neglected; then this equation has a solution satisfying the last of the initial conditions in (7):

$$E_1(z) = \sqrt{S}\exp\left(\frac{g}{2}\,I_0 z\right)\exp\left(\mathrm{i}\varphi_1\right). \tag{10}$$

With the above E_0 and E_1, the last equation in (9) with $\Delta k_1 = 0$ can be represented in the form

$$\frac{\mathrm{d}E_2}{\mathrm{d}z} = \frac{g}{2}\,S\exp\left(gI_0 z\right)\left\{E_2 + \sqrt{I_0}\exp\left[\mathrm{i}(2\varphi_1 - \varphi_0)\right]\right\}, \tag{11}$$

and has the solution

$$\begin{aligned}
E_2(z) &= \left\{E_2(0) + \sqrt{I_0}\exp\left[\mathrm{i}(2\varphi_1 - \varphi_0)\right]\right\}\\
&\quad\times\exp\left[\frac{S}{2I_0}\exp\left(gI_0 z\right)\right] - \sqrt{I_0}\exp\left[\mathrm{i}(2\varphi_1 - \varphi_0)\right]\\
&\approx \sqrt{I_0}\left\{\exp\left[\frac{S}{2I_0}\exp\left(gI_0 z\right)\right] - 1\right\}\exp\left[\mathrm{i}(2\varphi_1 - \varphi_0)\right].
\end{aligned} \tag{12}$$

The first term in the right-hand side of (12) describes the exponential increase in $E_2(z)$ with the coordinate z, but the term added to the initial value $E_2(0)$ to describe the parametric seed radiation (equal to the pump wave amplitude in modulus) is much greater than the seed Raman radiation with the amplitude $E_2(0)$. The phase of the wave E_2 is then given by $\varphi_2 = 2\varphi_1 - \varphi_0$; then the generalized FWM phase becomes $\Psi_1 = 2\varphi_1 - \varphi_0 - \varphi_2 = 0$, which makes this Stokes FWM process radically different from the previous anti-Stokes one. This leads to a high-efficiency parametric energy transfer from the SRS pump wave to the second Stokes component, i.e., its parametric generation leads the Raman process and accompanies it. This may account for the decrease and convergence of the lasing thresholds of Stokes SRS components in the case of their parametric coupling.

In the general case of multiline SRS, the combination of coupled parametric processes is observed, in which each SRS component is simultaneously the signal wave of one FWM, the FWM pump wave of another FWM, and the idle wave of a third FWM. In this case, the full system of equations for the stationary multiline SRS with parametric coupling has the form

$$\begin{aligned}
\frac{\mathrm{d}E_j}{\mathrm{d}z} &= -\frac{g_j}{2}\frac{\lambda_{j+1}}{\lambda_j}\,E_{j+1}\left[E_{j+1}^*(E_j + \varepsilon E_{j-1})\right.\\
&\quad\left. + E_{j+1}E_{j+2}^*\exp\left(\mathrm{i}\Delta k_{j+1} z\right)\right] + \frac{g_{j-1}}{2}\,E_{j-1}\\
&\quad\times\left[E_{j-1}^*(E_j + \varepsilon E_{j-1}) + E_{j-1}E_{j-2}^*\exp\left(\mathrm{i}\Delta k_{j-1} z\right)\right],
\end{aligned} \tag{13}$$

where g_j is the SRS gain coefficient under the jth component pumping; in other words, the dispersion of the SRS gain coefficient is now taken into account. Spontaneous Raman scattering is more correctly taken into account not in the initial conditions, which now become zero for the Stokes and anti-Stokes waves, but by additional terms proportional to εE_{j-1} (with the seed coefficient $\varepsilon \ll 1$).

Representing the complex wave amplitudes as $E_j = A_j \exp(\mathrm{i}\varphi_j)$, where A_j are the real wave amplitudes and φ_j are their phases, we obtain the rate equation for the generalized phases of coupled FWM processes (with $\Psi_j = 2\varphi_j - \varphi_{j-1} - \varphi_{j+1} + \Delta k_j z$):

$$\frac{\mathrm{d}\Psi_j}{\mathrm{d}z} \approx A_j^2 \left(\frac{g_{j-1}}{2} \frac{\lambda_j}{\lambda_{j-1}} \frac{A_{j+1}}{A_{j-1}} - \frac{g_j}{2} \frac{A_{j-1}}{A_{j+1}} \right) \sin \Psi_j + \Delta k_j + g_{j-1} A_{j-1}^2 \frac{A_{j-2}}{A_j} \sin \Psi_{j-1} - g_j \frac{\lambda_{j+1}}{\lambda_j} A_{j+1}^2 \frac{A_{j+2}}{A_j} \sin \Psi_{j+1} \,. \tag{14}$$

Expression (14) is written for the generalized phase of the jth FWM process. The last two terms in the right-hand side of (14) describe the influence exerted on the jth process by the neighboring, $(j+1)$th and $(j-1)$th, processes (we neglect the relatively weak effect of the $(j \pm 2)$th processes), and the remaining terms account for the description of the jth process itself. Therefore, every FWM process in SRS is influenced by the two neighboring FWM processes, and five adjacent SRS components participate in it.

3. Numerical simulation of SRS with the parametric coupling of radiation components in the example of a $BaWO_4$ crystal

We solve system (13) numerically for different values of the wave mismatch $\Delta k_j L$ and the SRS gain increment $g_0 I_0 L$, where L is the length of the SRS medium. For the SRS medium, we take a $BaWO_4$ crystal [1] pumped by Nd:YAG laser radiation with the wavelength $\lambda_0 = 1.064$ μm: the Raman frequency is $\nu_R = 926\ \mathrm{cm}^{-1}$, and the SRS gain coefficient for each SRS component [10] is

$$g_j \approx \frac{11.5 \times 10^5 (\lambda_j^{-1} + \nu_R)}{(1.267 \times 10^9 - \lambda_j^{-2})^2} \,, \tag{15}$$

where the wavelength $\lambda_j = (\lambda_0^{-1} - j\nu_R)^{-1}$ is measured in [cm] and g_j in [cm W^{-1}]. To ensure the attainment of the highest level of SRS lasing in the Stokes wave for $g_0 I_0 L = 30$ [1] in the absence of parametric coupling with the anti-Stokes wave ($\Delta k_0 L \to \infty$), the seed coefficient in Eqns (13) was taken to be equal to $\varepsilon = 3 \times 10^{-6}$. A threefold increase or decrease in ε resulted in the same output parameters of calculations when the increment $g_0 I_0 L$ was changed by no more than 10%.

Figures 1 and 2 show the calculated lasing threshold increments for different Stokes components depending on the wave mismatch parameters. The threshold increments $(g_0 I_0 L)_{\mathrm{th}}$ correspond to a two-percent (intensity) efficiency of lasing of a given SRS component. Figure 1 shows the threshold increment for the first Stokes wave as a function of the wave mismatch parameter $\Delta k_0 L$. Figure 2 shows the threshold increments $(g_0 I_0 L)_{\mathrm{th}2,3,4}$ for the second, third, and fourth Stokes components (with respect to $(g_0 I_0 L)_{\mathrm{th}1}$) versus the wave mismatch parameter $\Delta k_1 L = \Delta k_2 L = \Delta k_3 L$ for the Stokes waves. As suggested by the calculations, the dependence depicted in Fig. 1 holds for any values of the wave mismatch parameters $\Delta k_1 L$, $\Delta k_2 L$, and $\Delta k_3 L$, and the dependences in Fig. 2, in turn, are valid for any value of the wave mismatch $\Delta k_0 L$.

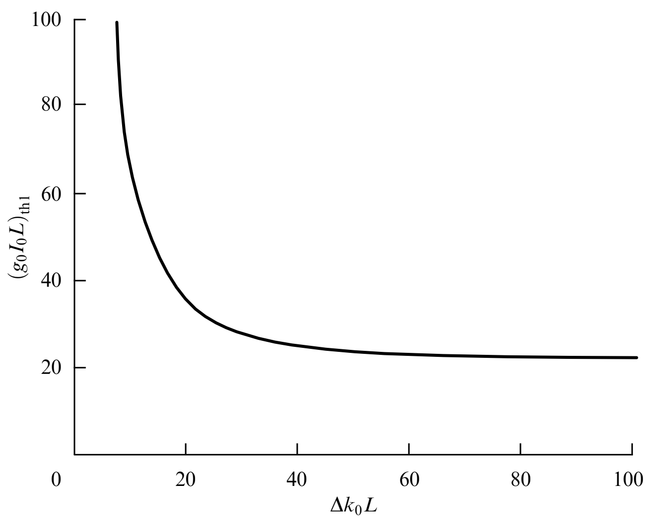

Figure 1. The calculated lasing threshold increment $(g_0 I_0 L)_{\mathrm{th1}}$ for the first Stokes component versus the parameter $\Delta k_0 L$ of the wave mismatch of the anti-Stokes wave for arbitrary mismatches $\Delta k_{1,2,3} L$ between the Stokes waves.

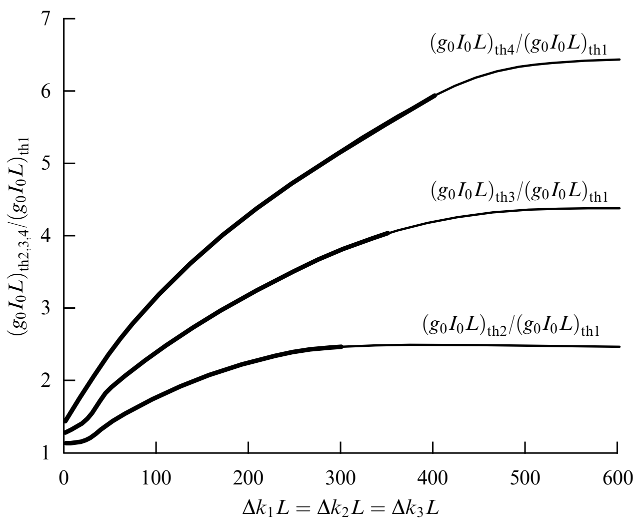

Figure 2. The calculated relative lasing threshold increments for the second $(g_0 I_0 L)_{\mathrm{th2}}/(g_0 I_0 L)_{\mathrm{th1}}$, third $(g_0 I_0 L)_{\mathrm{th3}}/(g_0 I_0 L)_{\mathrm{th1}}$, and fourth $(g_0 I_0 L)_{\mathrm{th4}}/(g_0 I_0 L)_{\mathrm{th1}}$ Stokes SRS components versus the parameter $\Delta k_1 L = \Delta k_2 L = \Delta k_3 L$ of the wave mismatch among the Stokes waves for an arbitrary mismatch $\Delta k_0 L$ of the anti-Stokes wave.

It can be seen from Fig. 1 that as the parametric coupling wave mismatch $\Delta k_0 L$ between the Stokes and anti-Stokes waves decreases, the Stokes wave lasing threshold tends to infinity for a zero argument, but the effect of this parametric coupling on the SRS conversion threshold already vanishes for $\Delta k_0 L > 50$, which gives the lowest value of the threshold increment, $(g_0 I_0 L)_{\mathrm{th1}} = 22$, in the absence of parametric coupling with the anti-Stokes wave. It follows from the dependence in Fig. 1 that ensuring low-threshold lasing by the first Stokes SRS component requires increasing $\Delta k_0 L > 50$ by choosing an SRS medium with a strong dispersion of the refractive index or with a long length L.

It can be seen from Fig. 2 that the parametric coupling between the Stokes components exerts an effect on the SRS conversion thresholds in a broader (by an order of magnitude) range of the wave mismatch $\Delta k_{1,2,3} L$ than in the case of anti-Stokes components, from zero to 200 – 500. However,

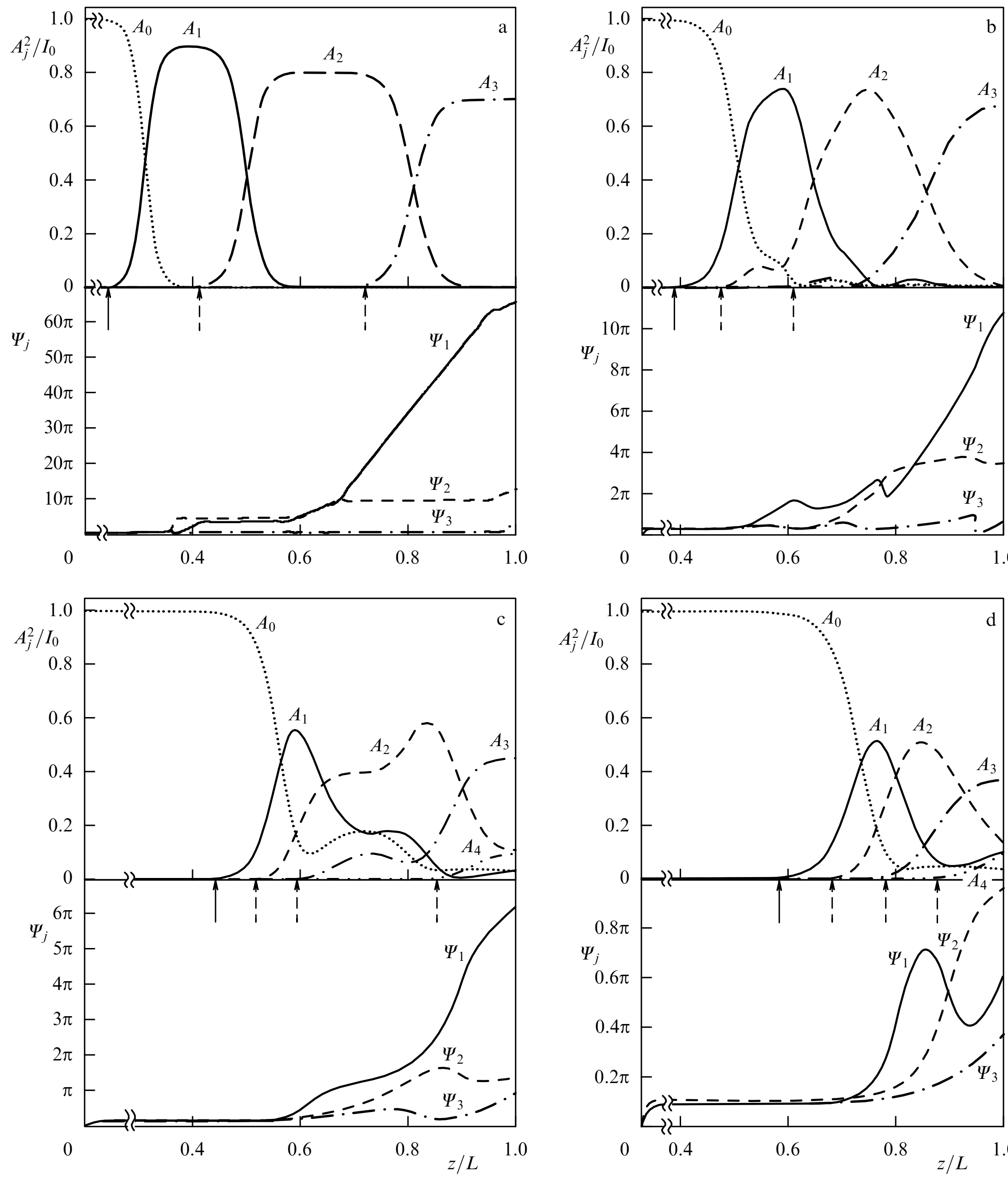

Figure 3. The calculated SRS component intensities and FWM-process phases as functions of the longitudinal coordinate for the highest intensity efficiency of the third Stokes component with $\Delta k_0 L = 500$ and $\Delta k_1 L = \Delta k_2 L = \Delta k_3 L = 200$ (a), 50 (b), 25 (c), and 10 (d).

the parametric coupling then decreases the SRS conversion thresholds, while the SRS conversion thresholds in the case of parametric coupling with the anti-Stokes wave, by contrast, are higher. The bold lines in Fig. 2 show the parts of the curves for which the calculations for a zero seed coefficient ($\varepsilon = 0$) yield coincident results for higher Stokes components of an order $j > 1$. In this case (for $\Delta k_1 L < 300$, $\Delta k_2 L < 350$, and $\Delta k_3 L < 400$), the initial generation of the higher Stokes waves is therefore purely parametric. The data shown in Fig. 2 allow concluding that the decrease in the lasing threshold for the higher Stokes wave of an order N requires imposing an additional constraint on decreasing $\Delta k_j L < 200$, where $j = 1, 2, \ldots, N - 1$. This may be realized in practice owing to the effect of normal dispersion of the refractive index ($n_0 > n_1 > n_2 > \ldots$) in solid SRS media in the visible and near-infrared ranges.

Figure 3 shows the solution results in the case of the highest lasing intensity efficiency of the third Stokes SRS component at the wavelength $\lambda_3 = 1.5$ μm for a completely weakened parametric coupling with the Stokes wave ($\Delta k_0 L = 500$) and four values of the wave mismatch between the Stokes waves: $\Delta k_1 L = \Delta k_2 L = \Delta k_3 L = 200$ (Fig. 3a), 50 (Fig. 3b), 25 (Fig. 3c), and 10 (Fig. 3d).

In Fig. 3a, which corresponds to the high value $\Delta k_{1,2,3} L = 200$ of the wave mismatch parameter (a strong dispersion and/or a long interaction length), the highest efficiency of the third Stokes component generation, $\eta_3 = A_3^2/I_0 = 0.704$, is observed for the high SRS gain increment $g_0 I_0 L = 82$, which calls for either a high pump power density or a long SRS medium–pump interaction length. This case is ordinarily realized in long glass–optical fiber SRS lasers or under intracavity pumping of SRS crystals. In this case, the thresholds for the first and second Stokes components differ by a factor of 1.8 and those for the first and third Stokes components by a factor of 3 (see the arrows on the horizontal axis).

For the small wave mismatch $\Delta k_{1,2,3}L = 10$ (Fig. 3d), which is realized closer to the domain of zero medium dispersion (for instance, $\lambda = 1.3$ μm for quartz fibers and $\lambda = 2.3$ μm for $PbMoO_4$ and $PbWO_4$ SRS crystals) or for a short interaction length L, the lasing thresholds for the first, second, and third Stokes components are found to be close to one another, and the requisite increment decreases to $g_0 I_0 L = 34.5$ (by a factor of 2.4). This favors the third component generation and obviates the necessity of resorting to high pump power densities close to the optical breakdown threshold of the SRS medium. But this is achieved at the cost of decreasing the SRS conversion efficiency from the quantum limit $(\lambda_0/\lambda_3)100\,\% = 70\,\%$ (Fig. 3a) to 37% (Fig. 3d), which can be generalized to the SRS generation of any higher Stokes components: the maximum generation efficiency decreases from λ_0/λ_j to $1/j$ as the parametric coupling becomes stronger. The reason for this lasing efficiency limitation lies with the early parametric generation of the next SRS component. The solution of the problem of lasing efficiency limitation may involve the introduction of selective losses into the SRS medium at the wavelength of the next Stokes component after the sought one, as was realized in Ref. [7], to obtain radiation with a record-long wavelength, $\lambda_4 = 3.69$ μm in a $BaWO_4$ crystal, where the next Stokes component fell into the range of strong absorption by the SRS crystal matrix.

We analyze the Raman-parametric conversion depicted in Fig. 3 in greater detail. Prior to depletion of the SRS pump (A_0), the generalized phases Ψ_j rapidly approach a constant level close to zero, because the increase in the ratio $A_j^2 A_{j-1}/A_{j+1}$ [see the first term in (14)] compensates the phase increase due to the wave mismatch Δk_j, but the greater Δk_j is, the greater the difference of a given phase level from the zero one and the lower the rate of initial parametric increase in A_j. Next, a rapid depletion of the SRS pump A_0 occurs due to the Raman ($A_0 \to A_1$) and parametric ($A_0 \to A_2$) transfer.

In Fig. 3a, parametric processes do not manifest themselves in the conversion of amplitudes because of a very large wave mismatch; but the domains of wave self-action and an increase in the phases $\Psi_{1,2,3}$ when $A_{1,2,3}$ peak, as well as an increase in $\Psi_1 \sim \Delta k_1 z$ upon the total depletion of the SRS pump can be observed in the phase curves. The Stokes SRS components sequentially peak in intensity (the well-known cascade-like character of SRS [17]); their peaks are plateau-like in shape, their relative (with respect to the input pump intensity) heights are λ_0/λ_j (j is the component order), and their widths increase with j due to a decrease in the SRS gain coefficient with increasing the wavelength [see formula (15)].

In Fig. 3b, the increase in Ψ_1 due to the self-action of A_0 and A_2 in the field of a strong wave A_1 proceeds more slowly, such that the initial parametric increase in A_2 is observed, but it rapidly becomes saturated to attain the initial 'parametric' maximum. The depletion of A_0 moderates, but the Raman transfer $A_0 \to A_1$ persists with the increase in A_1 up to its peak. This fosters the next Raman process $A_1 \to A_2$ with an increase in A_2 up to its main 'Raman' peak, whereby the self-action of A_0 and A_2 becomes weaker as Ψ_1 reaches a minimum of about π, resulting in a weak backward transfer $A_2 \to A_0$ with a low A_0 peak. Subsequently, the phase increases, $\Psi_1 \sim \Delta k_1 z$, because A_0 remains small, and the second term (Ψ_1) prevails in phase equation (14) for Δk_1. Next, the second parametric process $A_1 \to A_3$ sets in, which affects the first parametric process via the last term in phase equation (14) for Ψ_1. The increase in A_3 saturates the increase in the phase Ψ_1, which, on passing through a maximum, goes through a minimum and then, upon the complete depletion of A_0 and A_1, begins to increase proportionally to $\Delta k_1 z$ again. The self-action of A_1 and A_3 with an increase in Ψ_2 also rapidly terminates the parametric generation of A_3 (the initial 'parametric' peak of A_3) and its rapid increase occurs later (upon the attainment of the peak of A_2) as a result of the Raman transfer $A_2 \to A_3$ with the depletion of A_2.

In Figs 3c and 3d, the parametric processes manifest themselves even more strongly, such that the parametric peaks are even stronger than the Raman ones. In this case, the lasing thresholds of Stokes Raman components are determined by their parametric conversion and are substantially reduced (see the arrows on the horizontal axis).

For comparison, we outline several experimental results. Figure 4 shows the experimental data borrowed from Refs [22, 23] on the multistage generation of the first,

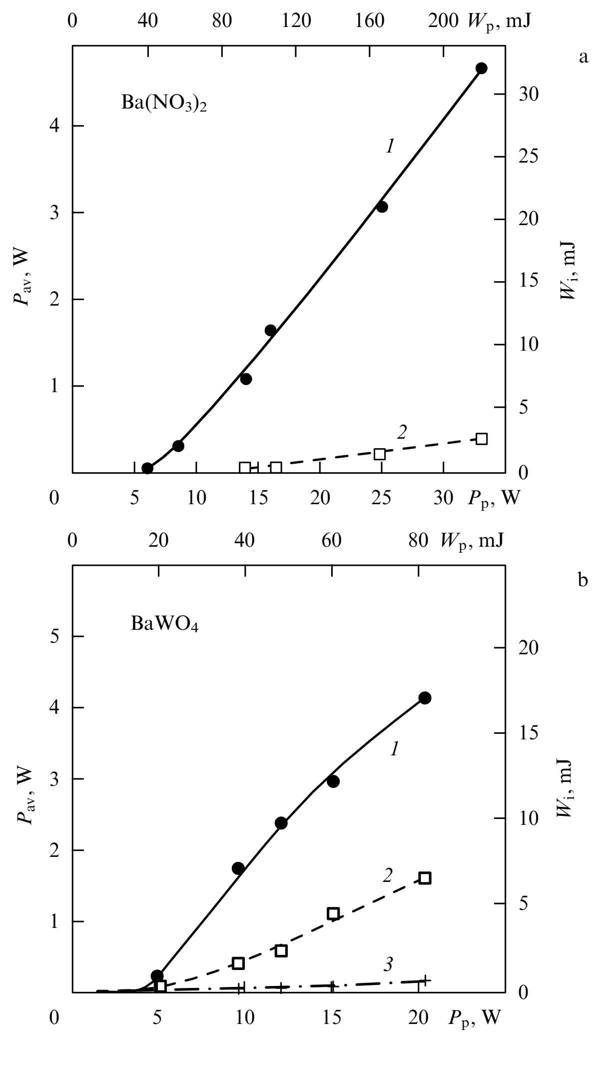

Figure 4. Experimental data borrowed from Refs [22, 23] on the multistage SRS generation of the first, second, and third Stokes components (lines *1*–*3*, respectively) in barium nitrate (a) and barium tungstate (b) crystals: P_{av} is the average output power; W_i is the output pulse energy; P_p is the average pump power; and W_p is the pump pulse energy.

second, and third Stokes components in the most promising SRS crystals $Ba(NO_3)_2$ and $BaWO_4$, pumped by $\lambda_0 = 1.064$ μm Nd:YAG laser radiation. It can be seen from the plots that the lasing thresholds of Stokes components in the $Ba(NO_3)_2$ crystal, which has a strong dispersion of the refractive index [24], are much different, which is an indication of a cascade-like process. By contrast, in the $BaWO_4$ crystal, which exhibits a weaker dispersion [25], the lasing thresholds of SRS components are quite close to each other and are lower than in the $Ba(NO_3)_2$ crystal, which is attributable to the strong parametric coupling of the SRS components. In the former crystal, only the first two Stokes components are effectively generated, and in the latter crystal, three components are generated (with a higher power than in the former case). The highest-order Stokes component with the wavelength $\lambda_3 = 1.5$ μm corresponds to the practically important radiation domain that is not harmful to the eye.

4. Summary

We have analyzed how the parametric processes of four-wave coupling of the frequency components in SRS in solids with dispersion depend on the wave mismatch of the four-wave mixing.

We have shown that the parametric coupling of the Stokes components affects the SRS conversion thresholds in a wider range (by an order of magnitude) of the wave mismatch $\Delta k_{1,2,3}L$ (from zero to $200-500$) than in the previously studied case of parametric coupling with the anti-Stokes wave. While the existence of parametric coupling of the anti-Stokes SRS components leads to an increase in the SRS threshold, the parametric coupling of the Stokes SRS components is responsible for the lowering and convergence of their lasing thresholds, which agrees nicely with experimental data.

It has been confirmed that ensuring a low-threshold lasing of the first Stokes component requires increasing the wave mismatch parameter to the anti-Stokes wave $\Delta k_0 L > 50$ by selecting SRS media with a strong dispersion $(\Delta k_0/\Delta\lambda_0)$ of the refractive index in the pump wavelength domain or with a long interaction length L (SRS in glass fiber lightguides or the intracavity pumping of SRS crystals). Decreasing the lasing threshold of the higher (second, third, and so on) Stokes waves requires the fulfillment of an additional condition for a decrease in the Stokes component wave mismatch parameters $\Delta k_j L < 200$, which may be realized in practice by choosing a nonlinear medium with a weak normal dispersion of the refractive index in the domain of the first, second, third, and higher-order Stokes waves, or by using a pump wavelength close to the edge of this domain.

Based on numerical simulations, we have analyzed the features of multiwave Raman-parametric conversion in the case of a significant depletion of the SRS pump radiation, the self-action of the waves, and the interplay of the neighboring processes of parametric four-wave mixing. The enhancement of the parametric coupling of Stokes waves has been shown to result in a sharp (more than twofold) reduction in requisite (threshold) SRS gain increments (and accordingly in the required pump power density) in comparison with those in the absence of parametric coupling. This permits realizing simpler and more reliable schemes for the SRS conversion of pump laser radiation for new wavelength ranges.

Acknowledgements. This work was supported in part by the Russian Foundation for Basic Research under grant No. 08-02-90479 and the Analytical Departmental Target Program "The Development of the Scientific Potential of Higher Educational Institutions" under project No. 2.1.1/3838.

References

1. Basiev T T *Usp. Fiz. Nauk* **169** 1149 (1999) [*Phys. Usp.* **42** 1051 (1999)]
2. Basiev T T et al., in *Solid-State Mid-Infrared Laser Sources* (Eds I T Sorokina, K L Vodopyanov) (Berlin: Springer, 2003)
3. Basiev T T, Powell R C, in *Handbook of Laser Technology and Applications* (Eds C E Webb, J D C Jones) (Bristol: Institute of Physics Publ., 2004)
4. Basiev T T, Osiko V V *Usp. Khimii* **75** 939 (2006) [*Russ. Chem. Rev.* **75** 847 (2006)]
5. Sushchinskii M M *Usp. Fiz. Nauk* **154** 353 (1988) [*Sov. Phys. Usp.* **31** 181 (1988)]
6. Kaminskii A A et al. *Usp. Fiz. Nauk* **178** 935 (2008) [*Phys. Usp.* **51** 899 (2008)]
7. Basiev T T et al. *Laser Phys. Lett.* **3** 17 (2006)
8. Zubov V A, Sushchinskii M M, Shuvalov I K *Usp. Fiz. Nauk* **83** 197 (1964) [*Sov. Phys. Usp.* **7** 419 (1964)]
9. Bloembergen N *Am. J. Phys.* **35** 989 (1967); *Usp. Fiz. Nauk* **97** 307 (1969)
10. Lisinetskii V A et al. *Laser Phys. Lett.* **2** 396 (2005)
11. Terhune R W *Bull. Am. Phys. Soc.* **2** 359 (1963)
12. Terhune R W *Solid State Design* **4** 38 (1963)
13. Loudon R *Proc. Phys. Soc. London A* **82** 393 (1963)
14. Garmire E, Pandarese F, Townes C H *Phys. Rev. Lett.* **11** 160 (1963)
15. Zeiger H J et al. *Phys. Rev. Lett.* **11** 419 (1963)
16. Bloembergen N, Shen Y R *Phys. Rev. Lett.* **12** 504 (1964)
17. Shen Y R, Bloembergen N *Phys. Rev.* **137** A1787 (1965)
18. Fabelinskii I L *Usp. Fiz. Nauk* **168** 1341 (1998) [*Phys. Usp.* **41** 1229 (1998)]
19. Butylkin V S et al. *Pis'ma Zh. Eksp. Teor. Fiz.* **17** 400 (1973) [*JETP Lett.* **17** 285 (1973)]
20. Andryunas K et al. *Pis'ma Zh. Eksp. Teor. Fiz.* **42** 333 (1985) [*JETP Lett.* **42** 410 (1985)]
21. Basiev T T et al. *Kvantovaya Elektron.* **14** 2452 (1987) [*Sov. J. Quantum Electron.* **17** 1560 (1987)]
22. Basiev T T et al. *Laser Phys.* **13** 1013 (2003)
23. Basiev T T et al. *Kvantovaya Elektron.* **34** 649 (2004) [*Quantum Electron.* **34** 649 (2004)]
24. Zverev P G et al. *Opt. Mater.* **11** 315 (1999)
25. Voronina I S et al. *J. Optoelectron. Adv. Mater.* **5** 887 (2003)
26. Born M, Wolf E *Principles of Optics* (Oxford: Pergamon Press, 1969) [Translated into Russian (Moscow: Nauka, 1970)]
27. Dmitriev V G *Nelineinaya Optika i Obrashchenie Volnovogo Fronta* (Nonlinear Optics and Phase Conjugation) (Moscow: Fizmatlit, 2003)
28. Shen Y R *The Principles of Nonlinear Optics* (New York: J. Wiley, 1984) [Translated into Russian (Moscow: Nauka, 1989)]